e-ISSN 2621-8062
Elipsoida : Jurnal Geodesi dan Geomatika
Vol 08 No 02, (2025)

MONITORING OF VERTICAL GROUND SURFACE MOVEMENT IN THE COASTAL AREA OF CILACAP REGENCY USING THE SMALL BASELINE SUBSET INTERFEROMETRY SAR (SBAS INSAR) METHOD

Luluk Sabdu Busoroh*, Hidayat Panuntun
Department of Earth Technology, Vocational School, Gadjah Mada University, Indonesia
e-mail: luluk.sabdu.busoroh@mail.ugm.ac.id*

(Received 07 July 2025, Accepted 26 November 2025, Published December 2025)

ABSTRACT

Cilacap Regency on the south coast of Java Island is prone to land movement due to its risky rock formation structure. Previous research found land subsidence in the coastal area of Cilacap District at -70 mm/year in the satellite view direction. The movement in the satellite view direction is not representative enough to show vertical movement directly. Thus, vertical movement in the coastal area of Cilacap Regency was calculated using the InSAR method. The data used is an unwrapped interferogram image of Sentinel-1 ascending and descending orbit from 2014 to 2024. Noise correction due to tropospheric delay is done with GACOS data. The data was processed using the Small Baseline Subset Interferometry SAR method with LiCSBAS software. Vertical movement was obtained via 2.5-D extraction from ascending and descending Line of Sight (LOS) displacement results and validated with GNSS CORS data of the CCLP station. The results show uplift on the south coast and subsidence in the northern part of Cilacap, with cumulative vertical displacement between -42.823 mm and 50.968 mm and velocities between -4.070 mm/year and 6.349 mm/year. Validation shows 2.5-D InSAR estimates are consistent with GNSS data.

Keywords : Vertical Displacement, InSAR, LiCSBAS, Time Series, Cilacap

1. INTRODUCTION

Vertical ground surface movement can be defined as changes in the position of the ground relative to a reference frame considered stable (Afif et al., 2018). Vertical surface movement includes both subsidence and uplift, which may occur gradually or suddenly (Fabiola & Panuntun, 2024). This phenomenon occurs in several regions of Indonesia, particularly in coastal areas (Iskandar et al., 2020). Coastal zones are highly vulnerable to land subsidence due to their fragile geological formations (Taufik et al., 2019). Cilacap Regency is one of the regions in Indonesia located along the southern coast of Java. Land use in the coastal area of Cilacap is dominated by dense urban settlements and rapid infrastructure development. In addition, Cilacap Regency is situated near the convergence zone between the Indo-Australian Plate and the Eurasian Plate. These conditions indicate that Cilacap has complex geodynamic characteristics influenced by the interaction between local geological conditions and anthropogenic pressures, both of which can trigger ground surface movement.

Ground movement is caused by two major factors: natural factors and human activities. Natural factors include soil conditions, geological structures, tectonic or volcanic activity, and collapses in limestone areas (Whittaker & Reddish, 1989). Several ground movement events are also induced by human activities such as excessive groundwater extraction, overproduction of oil and gas, improper land-use suitability, and excessive surface loading (Anugrah, 2020). These phenomena have various negative impacts, including coastal flooding (tidal inundation), land subsidence issues, sea-level rise, soil structure degradation, infrastructure and buildings damage (Fadhlurrohman et al., 2020).

One effort to minimize these impacts is through periodic ground movement monitoring. Ground deformation can be monitored using the Global Navigation Satellite System (GNSS) and Interferometric Synthetic Aperture Radar (InSAR). GNSS offers advantages such as continuous observation, weather independence, and millimeter-level accuracy (Khoirunisa et al., 2015). However, GNSS has limitations in spatial resolution because the measurements are point-based, meaning that it provides positional information only at the points without representing the overall surrounding area. This limitation makes GNSS less efficient for large-area monitoring, as it requires many stations. InSAR, on the other hand, provides an alternative solution because it offers high spatial resolution measurements. Similar to GNSS, InSAR can

achieve centimeter- to millimeter-level accuracy (Mahendra & Panuntun, 2022).

The InSAR method has been widely applied for monitoring ground surface deformation. A previous study conducted by Gultom (2017) utilized InSAR techniques to monitor surface movement in Central Java from 2015 to 2016. The study covered seven regions, including Cilacap, Pekalongan, Semarang, Demak, Gunung Kidul, Purwodadi–Blora, and Lasem. The results indicated signs of land subsidence in the coastal area of Cilacap with a rate of -70 mm/year relative to the satellite's Line of Sight (LOS). However, deformation measurements from either ascending or descending satellite orbits provide only one-dimensional displacement information based on the LOS direction (Mahendra & Panuntun, 2022). Observations from ascending and descending tracks may yield different results due to the difference in satellite viewing geometry during data acquisition.

Therefore, monitoring vertical ground surface movement by integrating both ascending and descending orbit data is necessary to determine the cumulative and rate of vertical deformation in the coastal area of Cilacap Regency. This study monitors land uplift and subsidence from 2014 to 2023. The research employs the Small Baseline Subset Interferometry SAR (SBAS-InSAR) method with 2.5-dimensional extraction to obtain more intuitive vertical displacement information compared to one-dimensional LOS-based deformation (Huang et al., 2016). This method extracts surface deformation from correlated SAR image series to produce a time series dataset (Berardino et al., 2002). The resulting time series is then used to identify vertical deformation patterns in the coastal region of Cilacap Regency.

2. DATA AND METHODS

2.1 Data

The primary data used in this study consist of unwrapped interferograms and coherence values from Sentinel-1 SAR imagery in GeoTIFF format, acquired from ascending mode (Frame ID 025A_09718_120810) and descending mode (Frame ID 076D_09725_121107) over the observation period from December 2014 to January 2024. These data were obtained from the COMET-LiCS portal (https://comet.nerc.ac.uk/COMET-LiCS-portal/). The dataset covers the study area, which is the coastal region of Cilacap Regency, Central Java. Geographically, Cilacap is located between 108°40' E–109°30' E and 7°30' S–7°45' S.

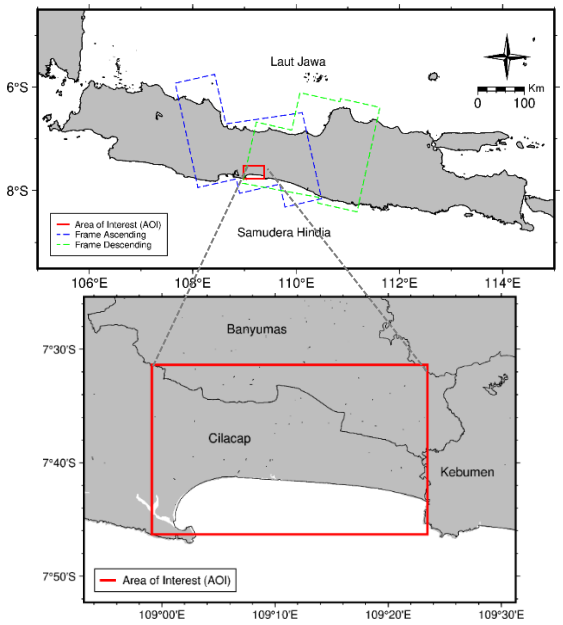

Figure 1. Research location

2.2 Methods

2.2.1 Small Baseline Subset Interferometry SAR (SBAS InSAR)

Small Baseline Subset (SBAS) is one of the InSAR time-series algorithms developed by Berardino et al. (2002). The SBAS method is an extension of the Differential Interferometric Synthetic Aperture Radar (DInSAR) technique, which utilizes phase differences between two SAR images to detect ground surface changes. However, DInSAR has limitations in monitoring long-term deformation because it is highly sensitive to atmospheric disturbances and temporal decorrelation. To address these limitations, SBAS employs multiple pairs of SAR images to detect small-scale surface deformation within an area with high accuracy. The formation of interferograms in the SBAS method is based on selecting image pairs with relatively short baselines to reduce spatial decorrelation and topographic errors (Berardino et al., 2002). The fundamental principle of the SBAS algorithm begins with selecting pairs of SAR images with small spatial and temporal baselines to generate a set of interferograms. Coherent pixels are identified by analyzing coherence maps computed alongside the interferograms. The next process is phase unwrapping to retrieve the original phase information from the interferogram. The unwrapped interferograms are then used to estimate surface deformation by separating deformation signals from

topographic and atmospheric disturbances using spatiotemporal filtering (Li et al., 2022). The final output of the SBAS processing is a deformation time series that can be used for further analysis (Casu et al., 2006).

2.2.2 Time Series Processing

This study uses the LiCSBAS software to process the SAR data. The LiCSBAS workflow begins with converting the GeoTIFF unwrapped interferogram files (.unw) into floating-point (float32) format and coherence files (.cc) into uint8 format. The next step is atmospheric correction using GACOS (Generic Atmospheric Correction Online Service) data to improve the quality of the interferograms. To filter out low-coherence pixels, a mask unwrapping procedure is applied using a coherence threshold of 0.1. The following step is clip unwrapping, which crops the area based on the Area of Interest (AOI) to accelerate subsequent processing steps. The next stage is data quality assessment using an unwrapping threshold of 0.5 and a coherence threshold of 0.05 to produce high-quality unwrapping results. This is followed by loop closure analysis, which aims to correct unwrapping errors by utilizing the redundancy of the interferogram network and phase loop closure. The loop phase value should be close to zero when the interferogram contains no unwrapping errors (Morishita et al., 2020). The subsequent process is Small Baseline Inversion to calculate pixel deformation rates based on a series of interferograms. Standard deviation estimation is performed using the bootstrap method by applying random sampling to the cumulative displacement data. The final steps include time-series masking to filter pixels based on a defined quality threshold and time-series filtering to separate residual noise caused by tropospheric, ionospheric, or orbital errors using a spatiotemporal Gaussian kernel filter.

2.2.3 2.5-D Deformation Calculation

Surface deformation derived from InSAR cannot fully represent all three-dimensional displacement components. This limitation arises because Sentinel-1 satellites operate only in two orbit geometries: ascending and descending. Sentinel-1 travels in a near-polar orbit from north to south or vice versa, with an east–west viewing geometry. Since the satellite's orbital heading is nearly parallel to the north–south (N–S) direction, displacement components along the N–S axis are difficult to detect (Panuntun, 2021). When both the satellite and the ground target move along the N–S direction, the displacement cannot be clearly observed from the satellite's line of sight. As a result, the deformation components that can be estimated are limited to the east–west (EW) and vertical (UD) directions. This approach is commonly referred to as 2.5-D displacement and can be expressed using Equation 1 (Fuhrmann & Garthwaite, 2019).

$$\begin{pmatrix} v\ LOS_{asc} \\ v\ LOS_{des} \end{pmatrix} = \begin{pmatrix} -sin\ \theta_{asc} \cos \alpha_{asc} & cos\ \theta_{asc} \\ -sin\ \theta_{des} \cos \alpha_{des} & cos\ \theta_{des} \end{pmatrix} \begin{pmatrix} vE \\ vU \end{pmatrix} \quad (1)$$

θ represents the incidence angle, which is the angle formed between the satellite sensor and the target on the Earth's surface. α denotes the azimuth of the Line-of-Sight (LOS) vector. The vertical displacement is calculated using the least squares adjustment (LSA) principle, simplified without considering orbital errors, as shown in Equation 2 (Fuhrmann & Garthwaite, 2019).

$$y = A.x + e \quad (2)$$

Matrix y is the observation vector containing the Line-of-Sight (LOS) deformation values from the ascending and descending satellite tracks, as expressed in Equation 3. Matrix A in Equation 4 is the coefficient matrix consisting of the partial derivatives of LOS deformation with respect to the eastward (vE) and vertical (vU) components. Matrix x contains the parameters to be estimated, namely the eastward and vertical deformation rates, obtained through the solution shown in Equation 5.

$$y = \begin{pmatrix} v\ LOS_{asc} \\ v\ LOS_{des} \end{pmatrix} \quad (3)$$

$$A = \begin{pmatrix} \frac{\partial\ vLOS}{\partial\ vE} & \frac{\partial\ vLOS}{\partial\ vU} \end{pmatrix} \quad (4)$$

$$X = \begin{pmatrix} vE \\ vU \end{pmatrix} = (A^T A)^{-1} A^T Y \quad (5)$$

3. RESULTS AND DISCUSSION

3.1 Line of Sight (LOS) Displacement

Line of Sight (LOS) displacement is the output generated from the InSAR data processing using the LiCSBAS software, representing ground surface motion relative to the satellite's viewing direction. In the LiCSBAS workflow, the system automatically selects the reference pixel for deformation by identifying the most stable pixel defined as the pixel experiencing the smallest change during the observation period. In this study, LOS displacement from both ascending and descending orbits was used as input data for calculating vertical ground displacement through 2.5-D extraction. The results of the Line of Sight (LOS) displacement processing are visually presented in Figure 2.

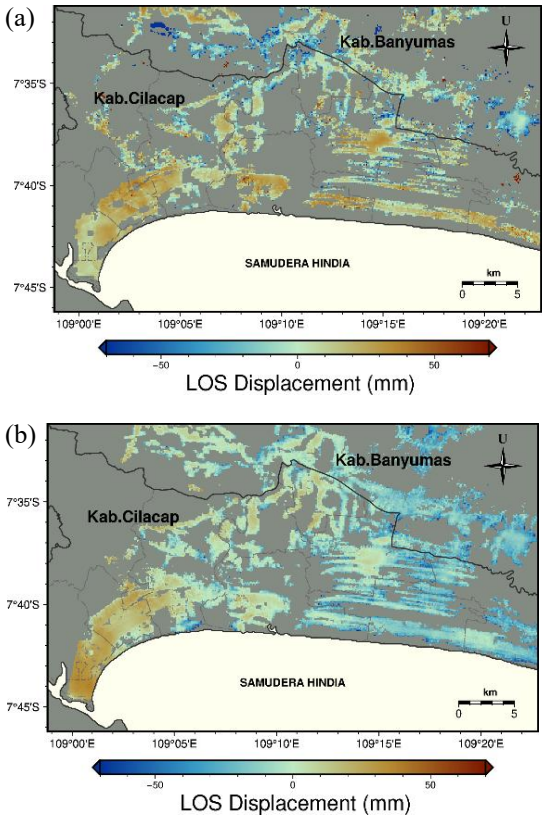

Figure 2. Relative cumulative displacement with respect to the satellite line of sight for (a) ascending orbit and (b) descending orbit

Table 1. Comparison of relative cumulative displacement with respect to the satellite line of sight and relative displacement velocity for the ascending and descending orbits.

Point	Relative Cumulative Displacement with Respect to the Satellite Line of Sight (mm)		Relative Displacement Velocity with Respect to the Satellite Line of Sight (mm/year)	
	Asc	Desc	Asc	Desc
1	33.04	39.74	4.547	4.368
2	44.67	23.01	6.424	2.848
3	-17.01	9.81	-0.379	0.244
4	-14.77	-23.73	-1.146	-2.524
5	35.40	13.90	4.205	2.201
6	13.09	18.28	1.877	2.339
7	-52.02	-1.66	-4.439	-0.149
8	27.95	10.20	3.867	1.929
9	27.48	-5.03	3.151	0.557
10	17.73	-17.29	1.330	-1.269
CCLP	2.58	41.66	1.021	4.446

The differences in cumulative displacement and relative displacement velocity with respect to the satellite's line of sight between the ascending and descending orbits are caused by variations in viewing geometry and differences in acquisition time. The viewing angle of the Sentinel-1 satellite when operating in Interferometric Wide Swath (IW) mode ranges from 31° to 46°. When the satellite observes ground objects from ascending and descending orbits, the viewing geometry differs between the two tracks, which may lead to variations in the interpreted displacement direction of the recorded objects. Differences in data acquisition time also influence the variation in LOS displacement results between the ascending and descending orbits. In addition, LOS displacement represents ground motion in a single dimension along the satellite's viewing direction. In reality, ground deformation occurs in three dimensions vertical, east–west, and north–south (Barone et al., 2025). Therefore, discrepancies between LOS displacement values from ascending and descending tracks can arise due to the contribution of horizontal components.

3.2 Vertical Displacement

Vertical displacement values were obtained through 2.5-D extraction from the Line-of-Sight (LOS) displacement data acquired from ascending and descending satellite tracks, processed using the LiCSBAS software. The 2.5-D extraction procedure combines ascending and descending observations to separate the vertical (U–D) and east–west (E–W) deformation components. The north–south (N–S) component can be neglected due to the limited diversity in viewing geometry and the low sensitivity of radar to motion in that direction (Wright dkk., 2004).

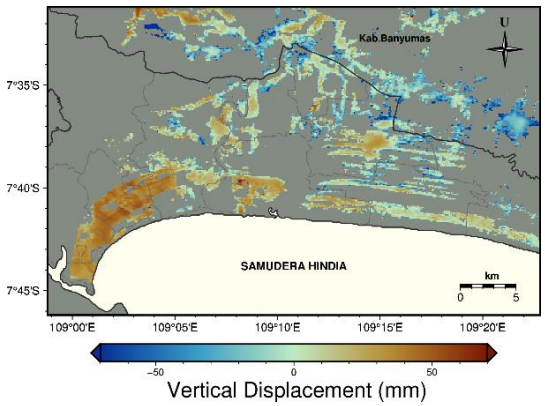

Figure 3. Cumulative vertical displacement

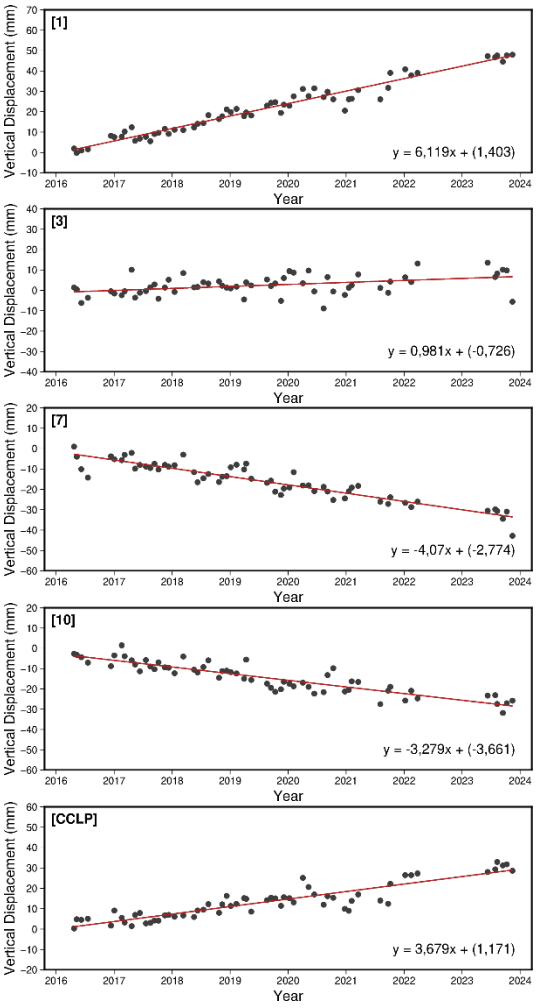

Figure 4. Vertical displacement time series

Based on the calculated vertical displacement, most sample points exhibit a clear sinusoidal pattern. This pattern is characterized by periodic upward and downward fluctuations in displacement over specific time intervals, producing a wavelike curve in the time-series graph. Such behavior indicates that ground motion at these points is not entirely accumulative but instead shows reversible movement that can return toward its initial state. This phenomenon is commonly associated with seasonal factors, such as variations in pore-water pressure driven by rainfall and dry-season conditions. In addition, sinusoidal patterns can be influenced by vegetation changes and radar signal disturbances caused by surface-condition variability.

Table 2. Cumulative vertical displacement and vertical displacement velocity

Point	Cumulative Vertical Displacement (mm)	Vertical Displacement Velocity (mm/year)
1	47.971	6.119
2	50.968	6.349
3	-5.601	0.981
4	-37.762	-3.614
5	30.867	4.333
6	18.512	2.332
7	-42.823	-4.070
8	27.989	4.195
9	15.943	2.478
10	-25.787	-3.279
CCLP	28.626	3.679

The deformation components obtained consist of cumulative vertical displacement and vertical displacement velocity. The cumulative vertical displacement values were derived from InSAR data processing, while the velocity values were obtained from the trend model. Based on Table 2, most sample points exhibit vertical movement with varying directions and magnitudes. Sample points 1 and 2 show the most significant ground uplift, with cumulative vertical displacement values of 47.971 mm and 50.968 mm, and velocities of 6.119 mm/year and 6.349 mm/year, respectively. Meanwhile, sample points 4 and 7 exhibit the largest subsidence, with cumulative displacement values of -37.762 mm and -42.823 mm, and subsidence rates of -3.614 mm/year and -4.070 mm/year, respectively. Sample points 3, 6, and 9 show relatively small displacement and velocity values, both in terms of uplift and subsidence. Overall, the results indicate that the southern coastal area of Cilacap exhibits a general tendency toward ground uplift during the observation period.

3.3 Spatial Distribution

Spatial distribution analysis is used to understand the pattern of vertical displacement across the coastal area of Cilacap Regency. In the context of surface deformation analysis using InSAR data, spatial distribution aims to identify locations experiencing ground movement either uplift or subsidence across the entire study area.

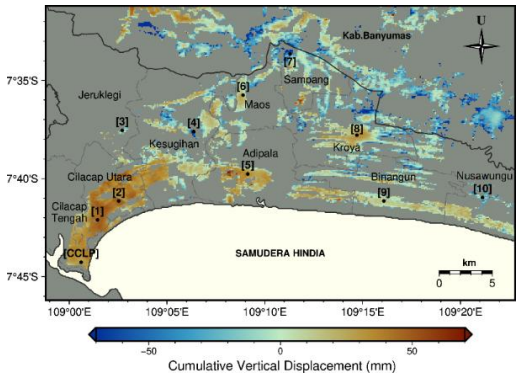

Figure 5. Spatial distribution of sample point locations

Variations in vertical ground displacement were detected in the coastal region of Cilacap Regency. Of the 10 observed districts, 6 experienced uplift and 4 experienced subsidence. The magnitude of uplift and subsidence at each sample point can be seen in Table 2. Observations from these data indicate a consistent pattern of ground uplift, particularly along the southern coastal area. This phenomenon is likely caused by strain accumulation due to tectonic activity. Indonesia lies within a complex tectonic setting, surrounded by three major plates: the Indo-Australian Plate, the Eurasian Plate, and the Pacific Plate. The Indo-Australian Plate moves northward and subducts beneath the Eurasian Plate, while the Eurasian Plate remains relatively stationary or moves very slowly toward the southeast (Bachri, 2014). The continuous northward movement and slow subduction of the Indo-Australian Plate beneath Java generate accumulated deformation, contributing to ground uplift along the southern coast of Java, including Cilacap Regency. When one zone experiences uplift due to tectonic force, the surrounding areas may undergo subsidence because the Earth's crust naturally bends to accommodate pressure changes.

3.4 Validation of InSAR Results Using GNSS Data

Validation of the processed results was performed by comparing vertical displacement values obtained from the SBAS InSAR method with field measurements from GNSS data. The GNSS data used for validation were collected from the CORS CCLP station located in Cilacap. This validation aims to assess the consistency of the InSAR-derived displacement results. GNSS data are selected as the reference because they provide high positional accuracy and direct measurements of ground movement.

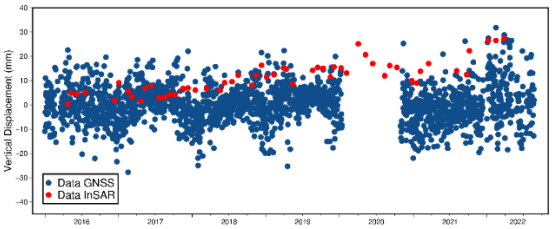

Figure 6. Time series plot of GNSS and InSAR data at CORS CCLP station for the period 2016–2022

Figure 6 shows a comparison of the vertical displacement time series derived from GNSS and InSAR observations at the CORS CCLP station from 2016 to 2022. Visually, both methods indicate a similar vertical displacement trend, characterized by a general uplift, although differences exist in data density and temporal continuity. InSAR data have lower temporal resolution compared to GNSS, yet the results demonstrate a relatively consistent trend throughout the observation period.

Table 3. Comparison of cumulative vertical displacement and vertical displacement velocity from GNSS and InSAR methods

Parameter	GNSS	InSAR
Cumulative Vertical Displacement (mm)	26.680	27.316
Vertical Displacement Velocity (mm/year)	2.636	3.216

Table 3 shows the consistency between the cumulative vertical displacement and the vertical displacement velocity obtained from both methods. This indicates that the InSAR data can accurately represent vertical ground movement within the study area. Overall, this validation strengthens the reliability of the SBAS InSAR processing results as an effective method for monitoring vertical surface displacement in the coastal region of Cilacap Regency.

4. CONCLUSIONS AND SUGGESTIONS

Based on the analysis results, the cumulative vertical displacement in the coastal area of Cilacap Regency during the period of 2015 to 2023 ranges from -42.823 mm to 50.968 mm, with annual vertical displacement rates varying between -4.070 mm/year and 6.349 mm/year. Spatially, the southern coastal region of Cilacap is predominantly characterized by ground uplift, while land subsidence occurs in the northern part of the study area. The uplift observed in the southern region is likely associated with tectonic activity, particularly the subduction of the

Indo-Australian Plate beneath the Eurasian Plate. This mechanism induces uplift along the coastal zone and subsidence in the northern inland area due to lithospheric bending. The InSAR processing results indicate that the highest uplift occurs in Cilacap Utara District, while the greatest subsidence is observed in Sampang District. Validation of the InSAR results with GNSS observations demonstrates that the 2.5-D vertical displacement estimates derived from LOS displacement are consistent with GNSS measurements.

In this study, InSAR data were validated only with GNSS measurements, resulting in the estimation of 2.5-D displacement. Future research is recommended to integrate both methods to obtain more comprehensive and accurate three-dimensional (3D) deformation information.

REFERENCES

Afif, M., Yuwono, D., & Awaluddin, M. (2018). Studi Penurunan Tanah Periode 2016-2017 Menggunakan Gamit 10.6 (Studi Kasus : Pesisir Kecamatan Sayung, Demak). *Jurnal Geodesi Undip Januari*, *7*(1). https://doi.org/10.6

Anugrah, C. (2020). *Analisa Penurunan Muka Tanah (Land Subsidence) Menggunakan Metode DInSAR di Kecamatan Pauh, Kota Padang, Sumatera Barat*. Skripsi, Institut Teknologi Padang.

Bachri, S. (2014). Pengaruh Tektonik Regional Terhadap Pola Struktur dan Tektonik Pulau Jawa. *Jurnal Geologi dan Sumber Daya Mineral*, *4*, 215.

Barone, A., Fedi, M., Pepe, A., Mastro, P., Tizzani, P., & Castaldo, R. (2025). Inferring 3D Displacement Time Series Through InSAR Measurements and Potential Field Theory in Volcanic Areas. *Scientific Reports*, *15*(1). https://doi.org/10.1038/s41598-025-88006-3

Berardino, P., Fornaro, G., Lanari, R., & Sansosti, E. (2002). A New Algorithm for Surface Deformation Monitoring Based on Small Baseline Differential SAR Interferograms. *IEEE Transactions on Geoscience and Remote Sensing*, *40*(11), 2375–2383. https://doi.org/10.1109/TGRS.2002.803792

Casu, F., Manzo, M., & Lanari, R. (2006). A Quantitative Assessment of the SBAS Algorithm Performance for Surface Deformation Retrieval from DInSAR Data. Remote Sensing of Environment, https://doi.org/10.1016/J.RSE.2006.01.023

Fabiola, A., & Panuntun, H. (2024). Karakterisasi Pergerakan Vertikal Permukaan Tanah di Tuban, Jawa Timur dengan Data SAR Sentinel-1 Menggunakan Teknik Small Baseline Subset (SBAS) Interferometry SAR (InSAR). *Journal of Geospatial Science and Technology*, *2*(2), 1–13. https://doi.org/10.22146/jgst.v2i2.15055

Fadhlurrohman, B., Prasetyo, Y., & Bashit, N. (2020). *Studi Penurunan Muka Tanah di Kawasan Industri Kendal dengan Metode Permanent Scatterer Interferometric Synthetic Aperture Radar (PS InSAR) Menggunakan Citra Sentinel 1-A TAHUN 2014-2019* (Vol. 9, Nomor 2).

Fuhrmann, T., & Garthwaite, M. C. (2019). Resolving Three-Dimensional Surface Motion with InSAR: Constraints from Multi-Geometry Data Fusion. *Remote Sensing*, *11*(3). https://doi.org/10.3390/rs11030241

Gultom, I. F. (2017). *Studi Deformasi di Jawa Tengah dan Sekitarnya dengan Menggunakan Metode InSAR*. Skripsi, Institut Teknologi Bandung.

Huang, M. H., Tung, H., Fielding, E. J., Huang, H. H., Liang, C., Huang, C., & Hu, J. C. (2016). Multiple Fault Slip Triggered Above the 2016 Mw 6.4 MeiNong Earthquake in Taiwan. *Geophysical Research Letters*, *43*(14), 7459–7467. https://doi.org/10.1002/2016GL069351

Iskandar, S. A., Helmi, M., Widada, S., & Baskoro Rochaddi. (2020). Analisis Geospasial Area Genangan Banjir Rob dan Dampaknya pada Penggunaan Lahan Tahun 2020-2025 di Kota Pekalongan Provinsi Jawa Tengah. Dalam *Indonesian Journal of Oceanography*. http://ejournal2.undip.ac.id/index.php/ijoice/

Khoirunisa, R., Yuwono, B., & Wijaya, A. (2015). Analisis Penurunan Muka Tanah Kota Semarang Tahun 2015 Menggunakan Perangkat Lunak Gamit 10.5. *Jurnal Geodesi Undip*, *4*.

Li, S., Xu, W., & Li, Z. (2022). Review of the SBAS InSAR Time-Series Algorithms, Applications, and Challenges. Geodesy and Geodynamics, 13(2), 114–126. https://doi.org/10.1016/J.GEOG.2021.09.007

Mahendra, G., & Panuntun, H. (2022). Ekstraksi Deformasi Koseismik 2.5-D Menggunakan Data Multiple SAR Sentinel-1 (Studi Kasus Gempa Bumi Iran 14 November 2021). *JGISE: Journal of Geospatial Information Science and Engineering*, *5*(2), 40. https://doi.org/10.22146/jgise.78205

Morishita, Y., Lazecky, M., Wright, T. J., Weiss, J. R., Elliott, J. R., & Hooper, A. (2020). LiCSBAS: An Open-Source InSAR Time Series

Analysis Package Integrated with the LiCSAR Automated Sentinel-1 InSAR Processor. *Remote Sensing*, *12*(3). https://doi.org/10.3390/rs12030424

Panuntun, H. (2021). 2.5-D Surface Deformation Due to the 24 January 2020 Elazig, Turkey Earthquake Estimated by Multiple Sentinel-1 InSAR Data. *2021 7th Asia-Pacific Conference on Synthetic Aperture Radar (APSAR)*, 1–5.

Taufik, M., Mutiara Anjasmara, I., & Fahrudin Ulin, R. (2019). Analisis Penurunan Muka Tanah di Kabupaten Gresik Tahun 2015 hingga 2017 dengan Metode Ps-InSAR. *Geoid*, *15(1)*, 6. Diakses 23 Februari 2025 (https://journal.its.ac.id/index.php/geoid/article/view/1628)

Whittaker, B. N., & Reddish, D. J. (1989). *Subsidence Occurrence, Prediction and Control*. Amsterdam, Netherlands ; New York : Elsevier ; New York, NY, U.S.A. : Distributors for the U.S. and Canada, Elsevier Science Pub. Co.

Wright, T. J., Parsons, B. E., & Lu, Z. (2004). Toward Mapping Surface Deformation in Three Dimensions Using InSAR. *Geophysical Research Letters*, *31*(1). https://doi.org/10.1029/2003GL018827